RSC Advances

PAPER

View Article Online
View Journal | View Issue

Cite this: *RSC Adv.*, 2019, **9**, 14004

In situ synthesis of C-doped $BiVO_4$ with natural leaf as a template under different calcination temperatures†

Ruijie Yang,[ab] Rongshu Zhu, *[ab] Yingying Fan,[ab] Longjun Hu[ab] and Qianqian Chen[ab]

In this work, a series of C-doped $BiVO_4$ ($BiVO_4$-*T*) with natural leaf structures were synthesized by a dipping-calcination method with the leaf of Chongyang wood seedling as a template under different calcination temperatures. The structures and morphologies of $BiVO_4$-*T* were observed by FE-SEM observations. The doped carbon in $BiVO_4$-*T* was formed *in situ* from the natural leaf during the calcination process and the amount of doping could be regulated from 0.51–1.16 wt% by controlling the calcination temperature. It was found that the sample calcined at 600 °C ($BiVO_4$-600) with a C-doping content of 1.16 wt% showed the best photocatalytic degradation activity. After 120 min visible light irradiation, the photocatalytic decomposition efficiency of RhB for $BiVO_4$-600 is 2.2 times higher than that of no template $BiVO_4$. The enhanced photocatalytic performance is ascribed to the combined action of the unique morphology and doped-carbon. It is considered that the unique structures and carbon doping of $BiVO_4$-600 are in favor of the enhancement of visible light absorption, which was supported by UV-vis DRS. Furthermore, the C-doping can enhance the efficient separation and transfer of the photo-generated electron–hole pairs, as proved by PL measurements. This study provides a simple dipping-calcination method and found the best calcination temperature to fabricate a high-performance $BiVO_4$, which simultaneously achieves morphology and C-doping control in one step.

Received 12th March 2019
Accepted 10th April 2019

DOI: 10.1039/c9ra01875a

rsc.li/rsc-advances

1. Introduction

Semiconductor photocatalytic technology has been considered to be an ideal candidate in solving the problem of environmental pollution, owing to its high-performance in degrading and mineralizing organic pollutants.[1,2] Among various semiconductor photocatalysts, bismuth vanadate ($BiVO_4$) has received much attention due to its narrow band gap for visible light absorption, low toxicity, low cost, and good stability.[3–9] Nevertheless, the low charge transportation efficiency of pure $BiVO_4$ leads to a very poor separation rate of electron–hole pairs, severely hindering its practical applications.[5,8,10–12]

In recent years, researchers have made much effort to improve the charge transportation efficiency of $BiVO_4$ and enhance its photocatalytic activity.[4,13–17] Li *et al.* found that depositing noble metals and transition metal oxides on (010) and (110) facets of $BiVO_4$ single crystals, respectively, can effectively promote the separation rate of photo-generated carriers.[4] Besides, Shan *et al.* reported that the $BiVO_4$/BiOI p–n heterojunction showed significantly enhanced photocatalytic activity for Rhodamine B (RhB) degradation[18] and Zhang *et al.* reported Z-scheme CdS–Au–$BiVO_4$ with enhanced photocatalytic activity for organic contaminant decomposition.[5] There are also some efforts of optimizing the structure of $BiVO_4$ to improve its photocatalytic activity. For example, Fan *et al.* reported an 3D micro/nanoarchitectures $BiVO_4$, having enhancement of far red to near infrared solar photocatalysis, which was synthesized with butterfly wings as template.[19] Our previous work (Published to *Catal. Sci. Technol.*, https://doi.org/10.1039/c9cy00475k, attached to ESI†) synthesized an multi-level structure $BiVO_4$ by a dipping-calcination method with the leaf of Chongyang wood seedling as template, with the enhancement of the degradation ratio of RhB. In addition, doping with a suitable element, such as C, N, Si, P, Mo *etc.*, is another method to enhance the photocatalytic properties of $BiVO_4$.[20] For example, Xu *et al.* investigated carbon-doped $BiVO_4$ with enhancement of photocatalytic degradation prepared by a two-step hydrothermal synthesis method using polyvinylpyrrolidone K-30 as a template and L-cysteine as the carbon source.[21] Yin *et al.* fabricated C-doped $BiVO_4$ with hierarchical structures by a novel sol–gel method to improve the photocatalytic activity for water oxidation and organic matter degradation.[20] In order to simultaneously achieve the structure and C-doping control in one step, we design and fabricate C-doped

[a]*Shenzhen Key Laboratory of Organic Pollution Prevention and Control, Environmental Science and Engineering Research Center, Harbin Institute of Technology (Shenzhen), Shenzhen 518055, P. R. China*

[b]*International Joint Research Center for Persistent Toxic Substances, Harbin Institute of Technology (Shenzhen), Shenzhen 518055, P. R. China. E-mail: rszhu@hit.edu.cn*

† Electronic supplementary information (ESI) available. See DOI: 10.1039/c9ra01875a

$BiVO_4$ with natural leaf as template by controlling the calcination temperature.

In this study, a series of C-doped $BiVO_4$ ($BiVO_4$-*T*) were synthesized by a dipping-calcination method with the leaf of Chongyang wood seedling as template under different calcination temperature. The field emission scanning electron microscopy (FESEM), X-ray diffraction (XRD), thermogravimetric and differential scanning calorimetry analyzer (TG-DSC) and fourier transform infrared spectroscopy (FTIR) were used to characterize the morphology, crystalline structure, the content of carbon doping and chemical composition of the photocatalysts. The UV-vis diffuse reflectance spectroscopy (DRS) and the photoluminescence (PL) spectra were analyzed to investigated the light absorption properties and separation rate of photo-generated carriers of the photocatalysts. Furthermore, the activities of the photocatalysts were evaluated by the RhB photocatalytic degradations under visible light irradiation.

2. Experimental section

2.1 Materials

All chemicals were of analytical grade and used without further purification. 37% hydrochloric acid, 25% glutaraldehyde, $Bi(NO_3)_3 \cdot 5H_2O$, NH_4VO_3, glycerol, ethanol and 65% nitric acid, were purchased from Sinopharm Chemical Reagent Co., Ltd., China. Tetramethylammonium hydroxide (TMAH) was purchased from Shanghai Jingchun Industrial Co. Ltd., China.

2.2 Synthesis of photocatalysts

A series of C-doped $BiVO_4$ were synthesized by a dipping-calcination method[19,22] with the leaf of Chongyang wood seedling as template. In a typical procedure, the leaves were soaked in 2% glutaraldehyde phosphate buffer at 4 °C for 8 h, immersed in 5% hydrochloric acid for 3 h, and immersed in $BiVO_4$ impregnation solution for 4 d (0.1 g leaf, 180 mL $BiVO_4$ impregnation solution), successively. The $BiVO_4$ impregnation solution was prepared as our previous work (Published to *Catal. Sci. Technol.*, https://doi.org/10.1039/c9cy00475k, attached to ESI†). After that, the treated leaf was calcined in air for 6 hours at 400, 450, 500, 550, 600, 650 and 700 °C in a furnace, respectively. Then the obtained catalysts were assigned as $BiVO_4$-*T* ($BiVO_4$-400, $BiVO_4$-450, $BiVO_4$-500, $BiVO_4$-550, $BiVO_4$-600, $BiVO_4$-650 and $BiVO_4$-700).

For comparison, no template $BiVO_4$ was also synthesized. Put the $BiVO_4$ impregnation solution (the same as above) into oven to dry at 60 °C for 48 h until the water evaporated completely. Then calcined the residue at 600 °C for 6 h. After that, no template $BiVO_4$ was obtained.

2.3 Characterization

The morphologies of the prepared photocatalysts were investigated using a HITACHI SU1080 FE-SEM. The BET surface area was evaluated by a ASAP2020M+C constant volume adsorption apparatus with N_2 adsorption. The XRD measurements were carried out on a Rigaku D/max 2550 VB/PC X-ray diffractometer with Cu Kα radiation. The TG-DSC of the samples were detected by a Netzsch STA 449F3 synchronous thermal analyzer. The FTIR spectra were recorded on a Thermo Scientific Nicolet IS50 spectrometer using a 360 nm LED laser as the light source and the detection wavelength was 540 nm. The UV-vis DRS were measured with a SHIMADZU UV-2450 spectrometer equipped with an integrating sphere assembly, using $BaSO_4$ as the reference material. The PL spectra were recorded on a SHIMADZU RF5301PC by using the 380 nm line of a Xe lamp as the excitation source at room temperature.

2.4 Photocatalytic activity measurements

The photocatalytic activities of the samples were evaluated by the degradations of RhB under visible light irradiation. Briefly, 10 mg catalyst was added in the RhB solution (150 mL, 10 mg L^{-1}). A 350 W Xe lamp (Shenzhen Stone-lighting Opto Device Co., Ltd., China) was used as a simulated solar light source. Before turning on the light, the suspension was stirred for 60 min in the dark to obtain the adsorption–desorption equilibrium of the RhB on the surface of the photocatalyst. Then, the suspension was irradiated by the lamp under magnetic stirring. In the course of the reaction, withdrawing 2 mL suspension from the reaction vessel every 20 min. And then, removed the photocatalyst from the suspension by centrifugation. Finally, the concentration of RhB in the solution was monitored using a UV-vis spectrophotometer (SHIMADZU UV-2450).

3. Results and discussion

3.1 Characterization of catalysts

3.1.1 Morphology analysis. The macroscopic morphology of the series of C-doping $BiVO_4$ and no template $BiVO_4$ are illustrated in Fig. 1. Compared with the powdered form of no template $BiVO_4$, the appearance of all the C-doping $BiVO_4$ exhibit the natural leaf's shape and the overall color gradually deepened with the increase of calcination temperature, which

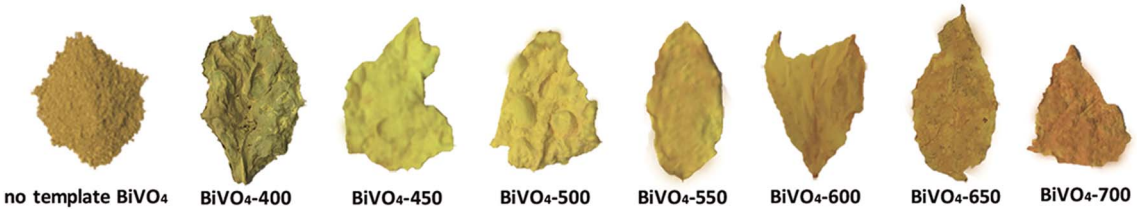

Fig. 1 The macrophotograph of no template $BiVO_4$, $BiVO_4$-400, $BiVO_4$-450, $BiVO_4$-500, $BiVO_4$-550, $BiVO_4$-600, $BiVO_4$-650 and $BiVO_4$-700.

Table 1 The carbon-doping contents and specific surface area of $BiVO_4$-*T* and no template $BiVO_4$

Catalyst	$BiVO_4$-400	$BiVO_4$-450	$BiVO_4$-500	$BiVO_4$-550	$BiVO_4$-600	$BiVO_4$-650	$BiVO_4$-700	No template $BiVO_4$
Carbon contents (wt%)	0.51	0.64	0.72	0.89	1.16	1.01	0.84	0
Specific surface area ($m^2\ g^{-1}$)	5.12	4.23	3.28	2.14	2.06	1.23	0.89	0.32

may be owing to the different amount of C-doping. In order to verify the carbon content, TG-DSC was carried out and the results are shown in Table 1. The C-doping content is increase from $BiVO_4$-400 at 0.51 wt% to $BiVO_4$-600 at 1.16 wt% and slightly decline when the calcination temperature exceeds 600 °C.

At the micro-level, the morphologies of C-doped $BiVO_4$ and no template $BiVO_4$ were observed by FE-SEM, shown in Fig. 2. In Fig. 2, compared with the cluttered distribution of $BiVO_4$ grain crystal for no template $BiVO_4$, the C-doped $BiVO_4$-*T* show the regular porous structures, which inherited from natural leaf's structure (the more leaf-liked structures has been observed in our precious work which has been published to *Catal. Sci. Technol.*, https://doi.org/10.1039/c9cy00475k, attached to ESI†). Moreover, from $BiVO_4$-400 to $BiVO_4$-700, the size of the crystallites gradually increase and the surface area (shown in Table 1) gradually decrease, illustrating that rising calcination temperature can make the grain size increase.

3.1.2 XRD analysis. The XRD of the different samples were analyzed to determine their crystallographic structures. Fig. 3 was the XRD patterns of the samples. As shown in Fig. 3A, all the catalysts exhibit the characteristic peaks of monoclinic scheelite phase $BiVO_4$ (JCPDS file: 14-0688),[12,23,24] implying that with increase in calcining temperature from 400 to 700 °C, the main crystalline phase of all the samples were monoclinic scheelite phase $BiVO_4$. It is worth noting that in the XRD pattern of

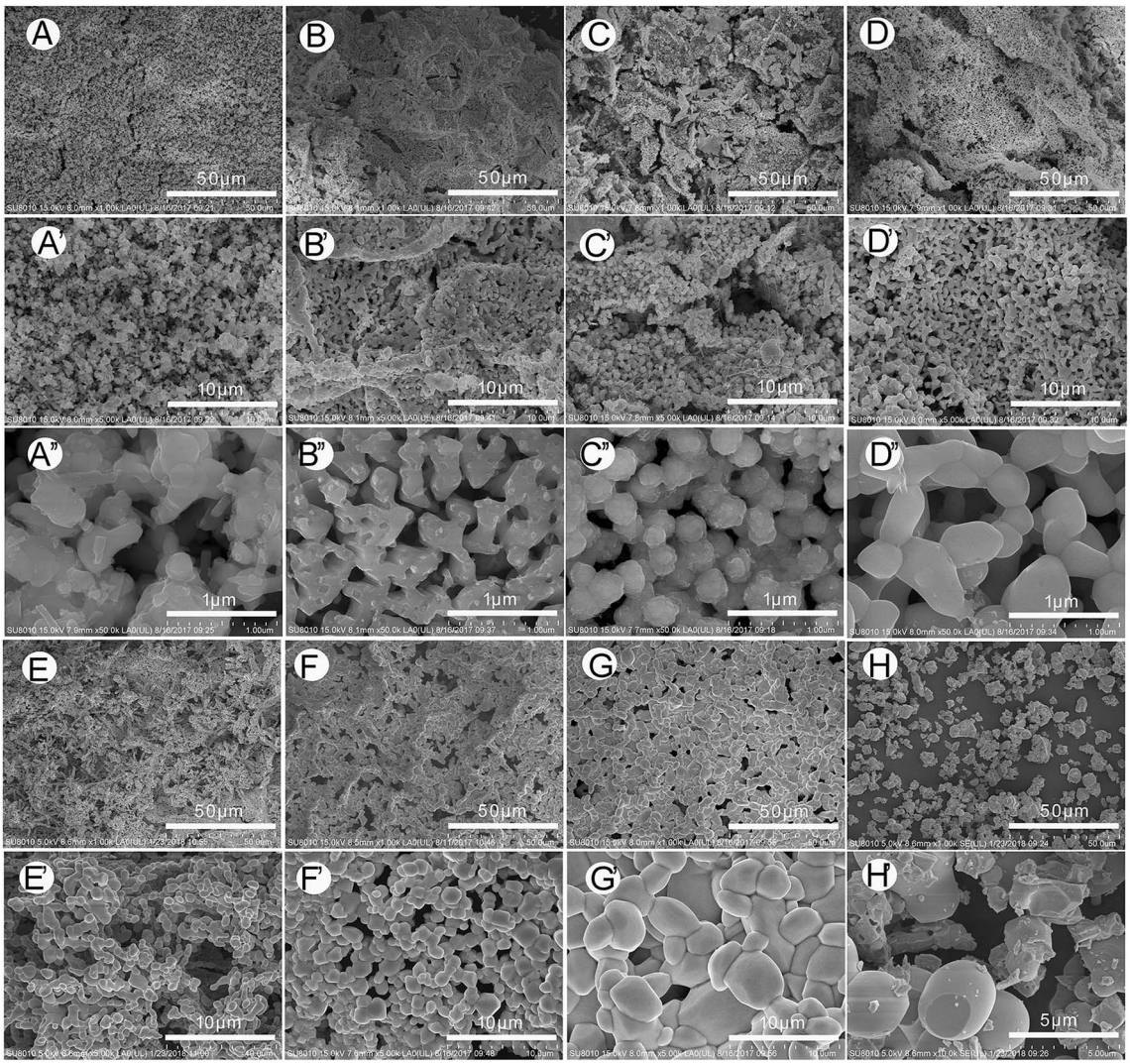

Fig. 2 FE-SEM images of $BiVO_4$-400 (A, A′ and A″), $BiVO_4$-450 (B, B′ and B″), $BiVO_4$-500 (C, C′ and C″), $BiVO_4$-550 (D, D′ and D″), $BiVO_4$-600 (E and E′), $BiVO_4$-650 (F and F′), $BiVO_4$-700 (G and G′) and no template $BiVO_4$.

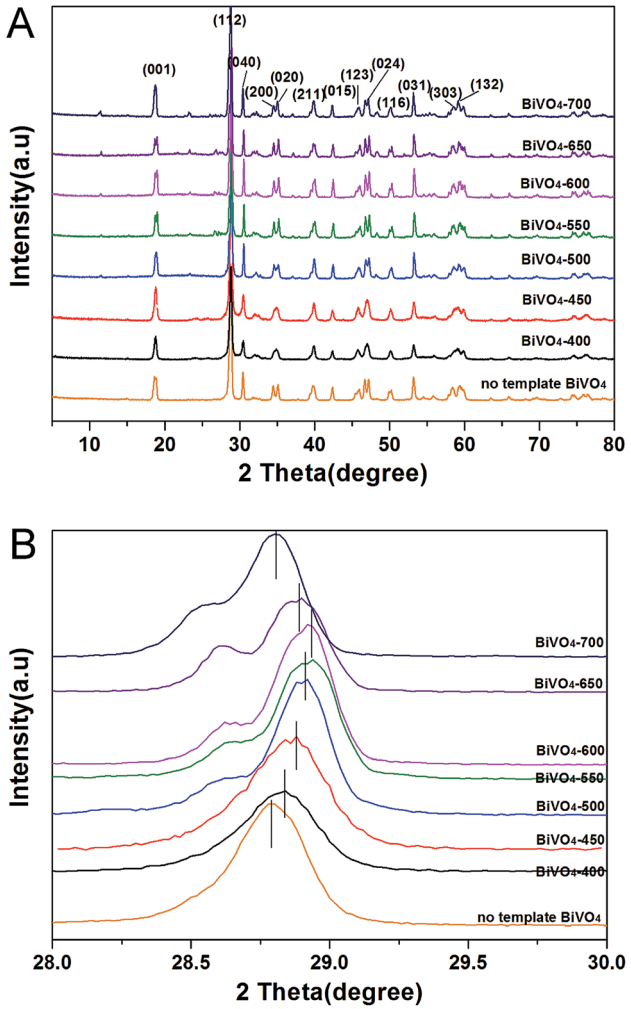

Fig. 3 XRD patterns (A) and magnified peaks of (112) planes in the range of 2θ from 28° to 30° (B) of no template $BiVO_4$, $BiVO_4$-400, $BiVO_4$-450, $BiVO_4$-500, $BiVO_4$-550, $BiVO_4$-600, $BiVO_4$-650 and $BiVO_4$-700.

$BiVO_4$-500, $BiVO_4$-550, $BiVO_4$-600, $BiVO_4$-650 and $BiVO_4$-700, there are some small peaks at a degree of 12, 23, 26, 38, 48, which can be assigned to the impurity phase $Bi_4V_2O_{11}$ (JCPDS file: 42-0135).[25] This results illustrated that when the calcination temperature reaches 500 °C, there will be some impurity phases. $Bi_4V_2O_{11}$ is an orthogonal compound, mainly a thermoelectric, ferroelectric material, and its photocatalytic performance is poor, mainly because its 3.05 eV band gap is difficult to excite in the visible range.[25] Fig. 3B shows a magnified view of (112) diffraction peaks, which exhibits gradual shifts to higher angles with the increase of calcination temperature and the peak drops back a little when the temperature exceed 600 °C. The maximum shifting of 0.125° is reached at $BiVO_4$-600, which having the largest amount of C-doping. Compared with (112) diffraction peak of no template $BiVO_4$, the peak of all the $BiVO_4$-*T* show higher angle shift. These result may be attributed to the lattice expansion owing to the slight part of carbon atom doping, and illustrates that C may have a certain influence on the *d*(121) spacings of the $BiVO_4$. It is considered that element doping is favor of the enhancement of photocatalytic activity for the incremental reactive sites and promoted electron–hole separation efficiency.[26]

3.1.3 FTIR spectra analysis. The FTIR spectra of $BiVO_4$-*T* and no template $BiVO_4$ are shown in Fig. 4. In the FTIR spectrums of all the samples, the absorption peaks at 475, 570, 736–744 and 840–845 cm^{-1} are corresponding to the typical symmetrical stretching vibration of VO_4^{3-}, stretching vibration of Bi–O, deformation bending vibration of V–O and symmetrical stretching vibration of V–O, respectively.[27,28] All absorption peaks at 3445 cm^{-1} are attributed to the stretching vibrations of the adsorbed H_2O. The absorption peak of $BiVO_4$-*T* at 1100 cm^{-1} is assigned to the typical antisymmetric stretching vibration of Si–O–Si,[29] while the peak is not appear in the FTIR spectra of no template $BiVO_4$, illustrating that the original Si element in the natural leaf doped into $BiVO_4$-*T*. Moreover, other methods has also been used to confirm the existence of Si, such as EDS (attached to the ESI†) and XPS (in our previous work, which has been published to *Catal. Sci. Technol.*, https://doi.org/10.1039/c9cy00475k, attached to ESI†).

3.1.4 UV-vis DRS analysis. The light absorption properties of the samples were analysed *via* UV-vis DRS, as shown in Fig. 5A. All of the samples have obvious absorption in range of visible light. For $BiVO_4$-400, $BiVO_4$-450, $BiVO_4$-500, $BiVO_4$-550 and $BiVO_4$-600, the absorption edge shows redshifts, while in case of $BiVO_4$-600, $BiVO_4$-650 and $BiVO_4$-700 there are blueshifts of the absorption edge. This regular change indicates that the band-gap energy of $BiVO_4$-*T* was affected by the calcination temperature, which is caused probably by the C doping. Moreover, the absorption edge of all C-doping $BiVO_4$-*T* show redshifts, compared with no template $BiVO_4$. This result may be attributed to the unique structures and C doping of $BiVO_4$-*T*.

The optical band gap of a semiconductor can be estimated according to the following formula:[29,30]

$$(\alpha h\nu) = A(h\nu - E_g)^{n/2}$$

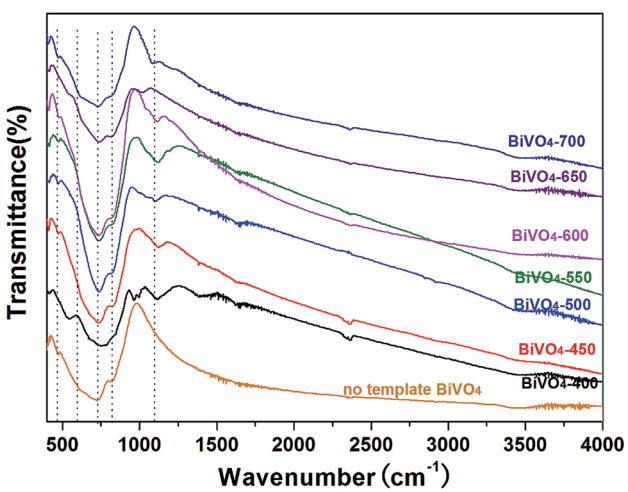

Fig. 4 FTIR spectra of no template $BiVO_4$, $BiVO_4$-400, $BiVO_4$-450, $BiVO_4$-500, $BiVO_4$-550, $BiVO_4$-600, $BiVO_4$-650 and $BiVO_4$-700.

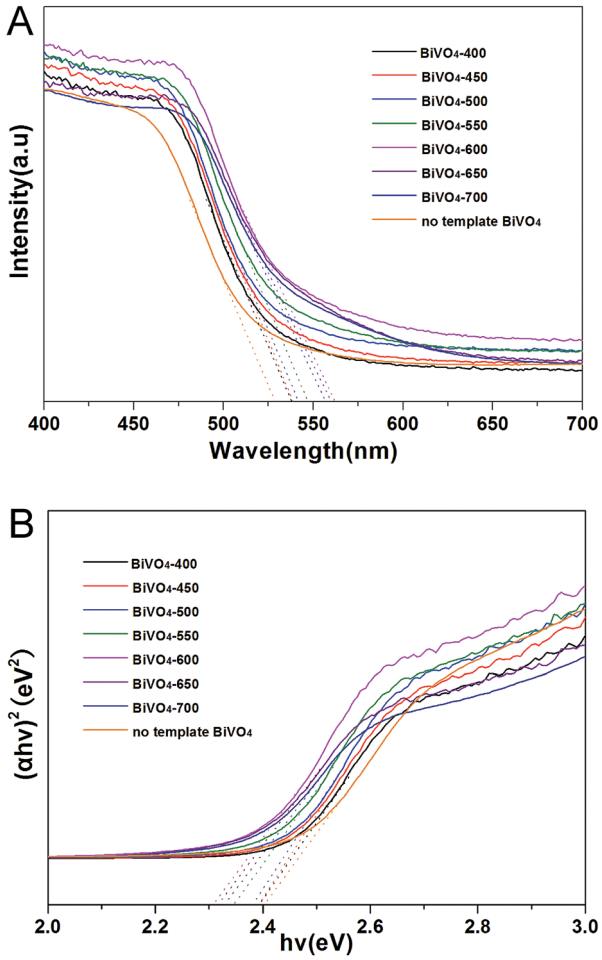

Fig. 5 (A) UV-vis DRS spectra of no template $BiVO_4$, $BiVO_4$-400, $BiVO_4$-450, $BiVO_4$-500, $BiVO_4$-550, $BiVO_4$-600, $BiVO_4$-650 and $BiVO_4$-700. (B) The calculation diagram of band gaps for no template $BiVO_4$, $BiVO_4$-400, $BiVO_4$-450, $BiVO_4$-500, $BiVO_4$-550, $BiVO_4$-600, $BiVO_4$-650 and $BiVO_4$-700.

where α, h, ν, A and E_g are absorption coefficient, Planck's constant, light frequency, constant value and band gap energy, respectively. Due to $BiVO_4$ are direct transition type of semiconductors, the direct band gaps of $BiVO_4$ can be calculated according to the plots of ($\alpha h\nu$) and *versus* ($h\nu$) (shown in Fig. 5B). Therefore, the band gap energy of no template $BiVO_4$, $BiVO_4$-400, $BiVO_4$-450, $BiVO_4$-500, $BiVO_4$-550, $BiVO_4$-600, $BiVO_4$-650 and $BiVO_4$-700 are determined to be 2.38, 2.40, 2.39, 2.38, 2.35, 2.31, 2.32 and 2.33 eV, respectively. It is clear that the banding gap energy shows a systematic decrease with the C doping level. Choi.[31] thought the electronic structure of the C–V bond and C–W bond are similar. Houston *et al.*[32] used to characterize the density state of the unfilled parts of the C–W guide band and found that the unfilled part of d orbit of C–W semiconductor is extending. In this work, there is a C–V bond in the catalyst, which has been confirmed in our previous work (Published to *Catal. Sci. Technol.*, https://doi.org/10.1039/c9cy00475k, attached to ESI†). Owing to the strong interaction between the orbit of V 3d and the C 2p, the minimum value of the guide band is further reduced, which is beneficial to the absorption of visible light.

3.1.5 PL analysis. Fig. 6 shows the PL spectra of $BiVO_4$-*T* and the no template $BiVO_4$. As shown in Fig. 6, all of the samples exhibit a strong PL emission peak around 540 nm, which can be attribute to the recombination of electro–hole pairs. The intensity of the peak gradually weaken with the calcining temperatures increase from 400 to 600 °C, while, as the temperature continues to increase from 650 to 700 °C, the intensity of the peak gradually enhance. In addition, compared with no template $BiVO_4$, all of the C-doped $BiVO_4$-*T* exhibit weaker PL intensity. The similar phenomena have also been observed in our previous studies,[3,33,34] which may be due to the doping of carbon element in favor of rapid electron transfer. Wang *et al.*[35] investigated the temporal evolution of fluorescence from carbon nanotubes and pointed out low fluorescence quantum yield originated from the rapidly quenching fluorescence rather than from the inherent weakness of the radiative transitions. Just because of high electron mobility, carbon affords the quick electron transfer resulting in the decrease of the emission intensity.

3.2 Photocatalytic activity

The photocatalytic activities of the samples were evaluated in terms of the degradations of RhB under visible light irradiation and shown in Fig. 7. For comparison, the blank experiment (no catalyst) was also performed. This result can exclude the effects of self-degradation of RhB under visible-light irradiation. After visible light irradiation for 2 h, the degradation ratio of RhB gradually increase from $BiVO_4$-400 at 47% to $BiVO_4$-600 at 82%. While, as the temperature continues to increase from 650 to 700 °C, the degradation ratio of RhB decrease slightly. $BiVO_4$-600 has the highest photocatalytic activity, suggesting that calcination temperature of 600 °C is optimized for the C-doped $BiVO_4$ photocatalyst.

It is generally considered that the catalytic performance is affected by morphology, crystallographic structure, chemical

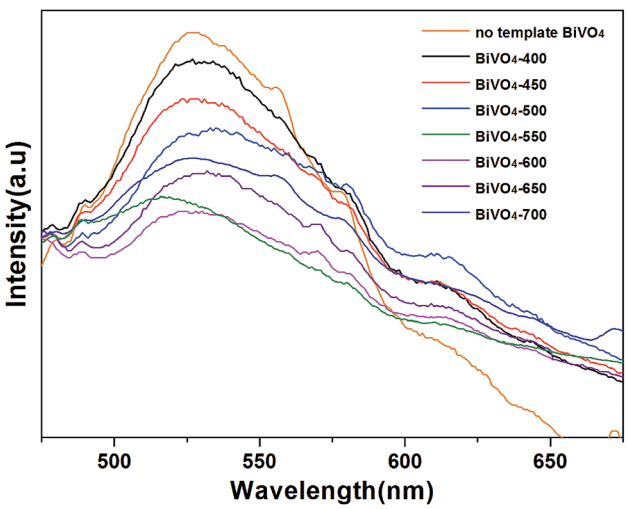

Fig. 6 PL spectra of no template $BiVO_4$, $BiVO_4$-400, $BiVO_4$-450, $BiVO_4$-500, $BiVO_4$-550, $BiVO_4$-600, $BiVO_4$-650 and $BiVO_4$-700.

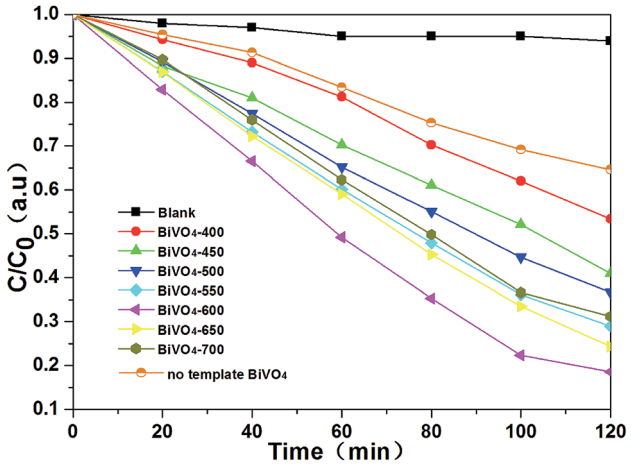

Fig. 7 Photocatalytic degradations of RhB over blank, no template $BiVO_4$, $BiVO_4$-400, $BiVO_4$-450, $BiVO_4$-500, $BiVO_4$-550, $BiVO_4$-600, $BiVO_4$-650 and $BiVO_4$-700.

composition, light absorption properties, and separation efficiency of the photo-generated electron–hole pairs of the semiconductor photocatalyst. However, in this work, with the increasing of calcining temperature, the morphology of the samples gradually deteriorate (the particle size gradually increase and the surface area gradually decrease), the crystallographic structures of all the samples were not changed (all the catalysts are monoclinic scheelite phase $BiVO_4$). Obviously, neither morphology nor crystallographic structures of the samples influences the photocatalytic activity. Comprehensively analyzing the photocatalytic activities of the photocatalysts and the UV-vis DRS and PL results, we can get that it is coincident that the regularities of the change of photocatalytic activities, the absorption edge and the separation efficiency of the photo-generated electron–hole pairs. Furthermore, according to the UV-vis DRS and PL analysis, all of the influence factor can be attribute to carbon element doping. With the rising of calcining temperature, the amount of doped carbon element increases and reaches optimum at 600 °C, $BiVO_4$-600 has the highest activity. While with the continually rise of calcining temperature, the amount of doped carbon element decreases, and the photocatalytic activity decreases with it. Therefore, The effect of calcination temperature on the catalytic activity of $BiVO_4$-*T* is mainly due to the influence of carbon doping content in the catalyst.

4. Conclusions

In this work, a series of C-doped $BiVO_4$ with natural leaf structures were synthesized by a dipping-calcination method with the leaf of Chongyang wood seedling as template under the calcination temperature of 400, 450, 500, 550, 600, 650 and 700 °C, respectively. The fine replication of natural leaf's macroscopic morphology and microstructure was confirmed directly by macrophotograph and FE-SEM. With the rise of calcination temperature, the carbon content of $BiVO_4$-*T* increase from $BiVO_4$-400 at 0.51 wt% to $BiVO_4$-600 at 1.16 wt%, while when the temperature exceed 600 °C, the carbon content drops back a little. The carbon doped into $BiVO_4$ crystal and induces lattice expansion. The measured photocatalytic activity results illustrate that $BiVO_4$-600 with a C-doping content of 1.16 wt% showed the best photocatalytic degradation activity. After 120 min visible light irradiation, the photocatalytic decomposition efficiency of RhB for $BiVO_4$-600 is 2.2 times higher than that of no template $BiVO_4$. The improved photocatalytic performance is ascribed to not only the leaf-liked structures but also the *in situ* doped-carbon, enhancing the visible light absorption ability as well as improving the separation of photo-generated electron–hole pairs. This study provides a simple dipping-calcination method and found the best calcination temperature to fabricate a high-performance $BiVO_4$, which simultaneously achieve the morphology and C-doping control in one step.

Conflicts of interest

There are no conflicts to declare.

Acknowledgements

All the authors gratefully acknowledge support from the Special Fund for the Development of Strategic and New Industry in Shenzhen (No. JCYJ20150731104949789) and the Fund for Knowledge Innovation in Shenzhen (No. JCYJ20180507183621817).

Notes and references

1 N. F. Moreira, J. M. Sousa, G. Macedo, A. R. Ribeiro, L. Barreiros, M. Pedrosa, J. L. Faria, M. F. Pereira, S. Castro-Silva, M. A. Segundo, C. M. Manaia, O. C. Nunes and A. M. Silva, *Water Res.*, 2016, **94**, 10–22.
2 J. Yu, P. Zhang, H. Yu and C. Trapalis, *Int. J. Photoenergy*, 2012, **2012**, 1–4.
3 M. Niu, R. Zhu, F. Tian, K. Song, G. Cao and F. Ouyang, *Catal. Today*, 2015, **258**, 585–594.
4 R. Li, H. Han, F. Zhang, D. Wang and C. Li, *Energy Environ. Sci.*, 2014, **7**, 1369–1376.
5 S. Bao, Q. Wu, S. Chang, B. Tian and J. Zhang, *Catal. Sci. Technol.*, 2017, **7**, 124–132.
6 Q. Wu, S. Bao, B. Tian, Y. Xiao and J. Zhang, *Chem. Commun.*, 2016, **52**, 7478–7481.
7 M. Zhou, H. B. Wu, J. Bao, L. Liang, X. W. Lou and Y. Xie, *Angew. Chem., Int. Ed. Engl.*, 2013, **52**, 8579–8583.
8 J. Tang, B. Song, Q. Deng and H. Xin, *Mater. Sci. Semicond. Process.*, 2015, **35**, 90–95.
9 S. M. Thalluri, C. Martinez Suarez, M. Hussain, S. Hernandez, A. Virga, G. Saracco and N. Russo, *Ind. Eng. Chem. Res.*, 2013, **52**, 17414–17418.
10 F. Lin, D. Wang, Z. Jiang, Y. Ma, J. Li, R. Li and C. Li, *Energy Environ. Sci.*, 2012, **5**, 6400–6406.
11 X. Gao, H. B. Wu, L. Zheng, Y. Zhong, Y. Hu and X. W. Lou, *Angew. Chem., Int. Ed. Engl.*, 2014, **53**, 5917–5921.

12 S. J. Hong, S. Lee, J. S. Jang and J. S. Lee, *Energy Environ. Sci.*, 2011, **4**, 1781.
13 D. Wang, R. Li, J. Zhu, J. Shi, J. Han, X. Zong and C. Li, *J. Phys. Chem. C*, 2012, **116**, 5082–5089.
14 J. Yang, D. Wang, X. Zhou and C. Li, *Chemistry*, 2013, **19**, 1320–1326.
15 D. Tang, H. Zhang, H. Huang, R. Liu, Y. Han, Y. Liu, C. Tong and Z. Kang, *Dalton Trans.*, 2013, **42**, 6285–6289.
16 W. Zhao, Y. Wang, Y. Yang, J. Tang and Y. Yang, *Appl. Catal., B*, 2012, **115–116**, 90–99.
17 C. Li, P. Zhang, R. Lv, J. Lu, T. Wang, S. Wang, H. Wang and J. Gong, *Small*, 2013, **9**, 3951–3956, 3950.
18 L. Shan, Y. Liu, J. Bi, J. Suriyaprakash and Z. Han, *J. Alloys Compd.*, 2017, **721**, 784–794.
19 R. Yan, M. Chen, H. Zhou, T. Liu, X. Tang, K. Zhang, H. Zhu, J. Ye, D. Zhang and T. Fan, *Sci. Rep.*, 2016, **6**, 20001.
20 C. Yin, S. Zhu, Z. Chen, W. Zhang, J. Gu and D. Zhang, *J. Mater. Chem. A*, 2013, **1**, 8367.
21 D. Zhao, W. Zong, Z. Fan, S. Xiong, M. Du, T. Wu, Y.-W. Fang, F. Ji and X. Xu, *CrystEngComm*, 2016, **18**, 9007–9015.
22 H. Zhou, J. Guo, P. Li, T. Fan, D. Zhang and J. Ye, *Sci. Rep.*, 2013, **3**, 1667.
23 M. Zalfani, B. van der Schueren, Z.-Y. Hu, J. C. Rooke, R. Bourguiga, M. Wu, Y. Li, G. Van Tendeloo and B.-L. Su, *J. Mater. Chem. A*, 2015, **3**, 21244–21256.
24 C. Lv, G. Chen, J. Sun, C. Yan, H. Dong and C. Li, *RSC Adv.*, 2015, **5**, 3767–3773.
25 Y. Shen, M. Huang, Y. Huang, J. Lin and J. Wu, *J. Alloys Compd.*, 2010, **496**, 287–292.
26 Q. Yun, A. Bai and S. Zhao, *J. Rare Earths*, 2014, **32**, 884–889.
27 J. Liu, H. Wang, S. Wang and H. Yan, *Mater. Sci. Eng., B*, 2003, **104**, 36–39.
28 A. Zhang and J. Zhang, *Spectrochim. Acta, Part A*, 2009, **73**, 336–341.
29 X. Wu, J. Zhao, L. Wang, M. Han, M. Zhang, H. Wang, H. Huang, Y. Liu and Z. Kang, *Appl. Catal., B*, 2017, **206**, 501–509.
30 B. Weng, S. Liu, N. Zhang, Z.-R. Tang and Y.-J. Xu, *J. Catal.*, 2014, **309**, 146–155.
31 J.-G. Choi, *J. Catal.*, 1999, **182**, 104–116.
32 J. E. Houston, G. E. Laramore and R. L. Park, *Science*, 1979, **185**, 258–260.
33 F. Tian, R. Zhu, J. Zhong, P. Wang, F. Ouyang and G. Cao, *Int. J. Hydrogen Energy*, 2016, **41**, 20156–20171.
34 R. Zhu, F. Tian, S. Che, G. Cao and F. Ouyang, *Renewable Energy*, 2017, **113**, 1503–1514.
35 F. Wang, G. Dukovic, L. E. Brus and T. F. Heinz, *Phys. Rev. Lett.*, 2004, **92**, 177401.